Chapter 16

# The Physics of Weld Bead Defects

P. S. Wei

Additional information is available at the end of the chapter

http://dx.doi.org/10.5772/50668

## 1. Introduction

Productivity in different welding techniques can be improved by increasing welding speed and current. This strategy, however, is limited by the appearance of surface defects such as rippling, humping, undercutting, etc [1]. Weld ripples exhibit rather regular, arc-shaped topographic features on a solidified surface, for example, as shown in Figure 1 in EBW of Al 6061 [2]. The ripples slightly elevate above the surface. Figure 2 shows a rippling structure on silicon surface irradiated by a p-polarized laser beam, provided by Pedraza et al. [3]. Notice tiny little "fingers" in lower rim of fringes and asymmetry in fringe profile taken in downward direction.

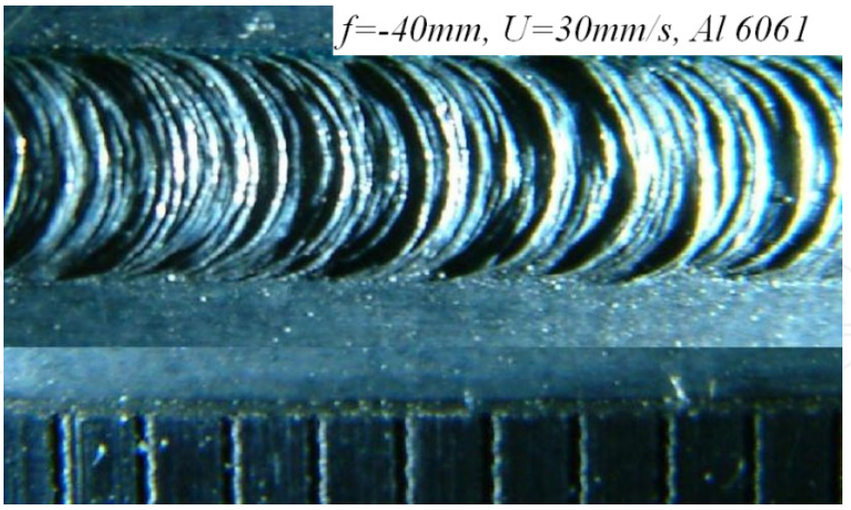


**Figure 1.** Rippling in welding Al 6061 [2]

On the other hand, more complicated humping shows an irregular and unpredictable surface contour consisting of a series of swelled protuberance, as can be seen in Figures 3(a)-(d). Morphologies of humped welds are quite complicated, which were roughly categorized into the gouging region and beaded cylinder morphologies [4]. Typical gouging region

morphology defects in GTAW at high currents and high travel speeds are shown in Figure 3(a) [5]. The front of the weld pool exhibits a large depression known as the gouging region. Open, unfilled dry spots in between the humped beads can also be seen. In some cases, two small channels appear at the walls of the gouging region. The weld bead having parallel grooves at the side is the undercutting defect.

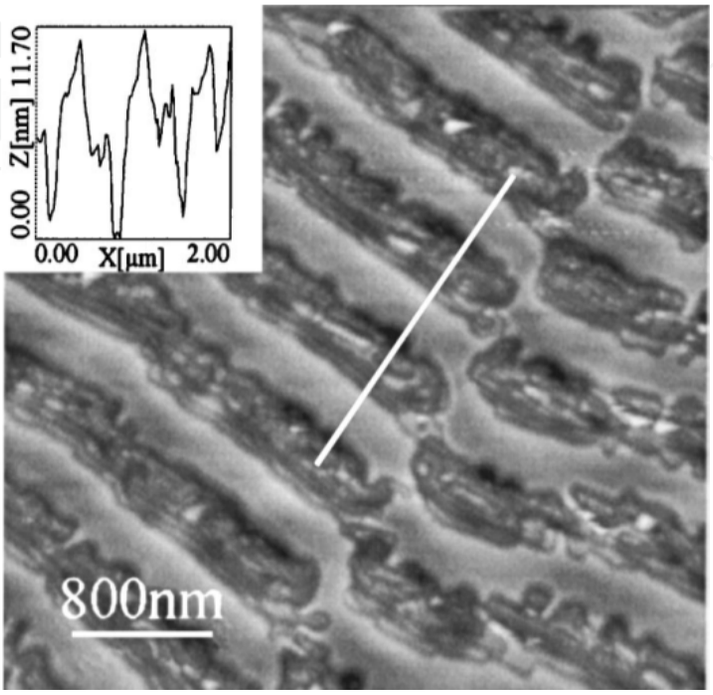


**Figure 2.** Rippled structure irradiated by 50 pulses at a laser fluence of 0.7 $J/cm^2$, using a p-polarized beam and incident angle of $38.5^\circ$. Notice "fingers" in lower rim of fringes [3].

Figure 3(b) shows a parallel humping or a split bead, separated by an empty channel [5]. Figure 3(c) shows beaded cylinder morphology defects, which are quite different from the gouging region morphology [6]. The beaded cylinder morphology includes beadlike protuberances that sit above the workpiece surface and are connected by a narrow central channel. In some cases of disconnected protuberances, traces of a central channel can still be seen. It is interesting to find that the gouged region and bead cylinder morphology are inverse phenomenon. Different morphologies therefore can be revealed by simply interchanging the liquid and gas phases. Figure 3(d) shows humping in EBW of Al 5083 [2]. Figure 4 also shows the a "star-like" or finger structure develops as well as the number of rays increases with laser power in etching of regular holes in Mo films with an $Ar^+$ laser beam immersed in $Cl_2$ atmosphere [7]. Surface patterns of weld beads therefore are very complicated.

Even though formation of the defects have been extensively proposed in the past, more systematical understanding of pattern formations is still limited. The aims of this work are to provide rigorous and pictorial interpretation based on thermal science concepts, and clarify and propose some physics involved in the mechanisms of weld bead formation. Clear physical concepts associated with quantitative scale analysis are important and beneficial for predicting, controlling and avoiding the occurrence of surface defects [1].

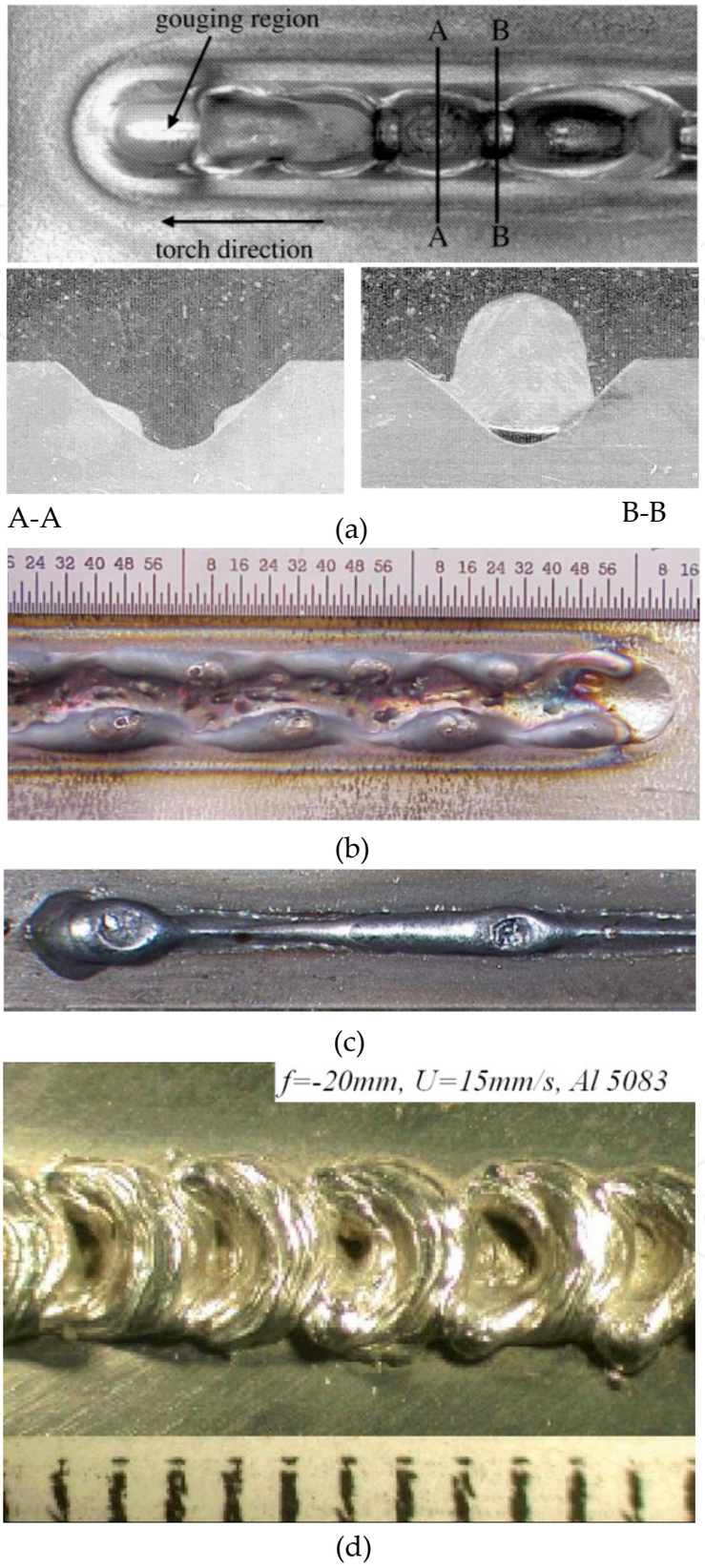


**Figure 3.** (a) Humps with gouged region and (b) parallel hump in GTAW [5], (c) cylinder beads in GMAW [6], and (d) humps in EBW [2].

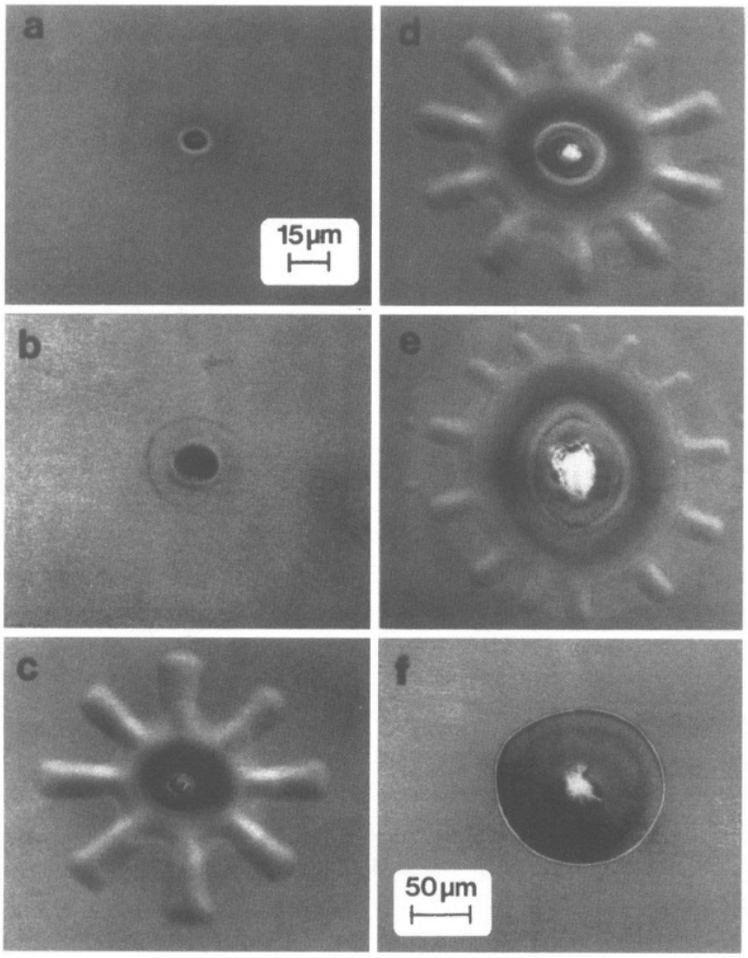


**Figure 4.** A "star-like hole" in etching Mo films with an $Ar^+$-laser in $Cl_2$ atmosphere with powers (a) 10 mW, (b) 20 mW, (c) 50 mW, (d) 100 mW, (e) 500 mW, and (f) 150 mW [7].

## 2. Mechanisms of surface patterns

Different mechanisms of rippling have been proposed and summarized in Table 1.

| | |
|---|---|
| Solidification rate fluctuations | Cheever and Howden [8], D'annessa [9] |
| Power source effects | Garland and Davies [10], Ecer et al. [ 11] |
| Thermocapillary instability | Fujimura et al. [ 12] |
| Kelvin-Helmholtz instability | Ang et al. [13] |
| Rayleigh-Taylor instability | Bennett et al. [14], Lugomer [15] |
| Instability due to evaporation | Emel'yanov et al. [16] |
| Morphological instability | Weizman et al. [17], Style and Wettlaufer [ 18] |
| Thermocapillary edge flow | Anthony and Cline [19], Wei et al. [20, 21] |
| Laser interactions | Birnbaum [22], Siegman and Fauchet [ 23] |

**Table 1.** Mechanisms proposed for rippling

On the other hand, different mechanisms responsible for humping are presented in Table 2.

| | |
|---|---|
| Rayleigh's capillary instability | Bradstreet [24], Gratzke et al. [25], Albright and Chiang [26] |
| Kelvin-Helmholtz instability | Kumar and DebRoy [27], Tytkin et al. [28] |
| Hydraulic jump | Shimada and Hoshinouchi [29] |
| Thermocapillary edge flow | Wei [1] |

**Table 2.** Mechanisms proposed for humping

| | |
|---|---|
| Kelvin-Helmholtz instability | Dynamic pressure difference |
| Rayleigh-Taylor instability | Density difference |
| Rayleigh capillary instability | Capillary pressure difference |
| Morphological instability | Solute supersaturation |
| Thermocapillary instability | Surface tension gradient |
| Evaporation instability | Evaporation pressure difference |
| Hydraulic jump | Hydraulic pressure difference |
| Laser interaction | Polarizations |
| Gravitational-electromagnetic instability | Interactions between gravitational and electromagnetic forces |

**Table 3.** Mechanisms of instabilities

Surface roughness including rippling, gouging, humping, fingers, etc., therefore can be affected by mechanisms shown in Table 3. Understanding their physical meanings is described as follows.

## 3. Thermal science analysis of surface patterns

Rippling or humping is determined by the formation of capillary wave on the free surface. Under surface tension, the pressure differences created at a curve interface support deformation of the interface, as sketched in figure 5.

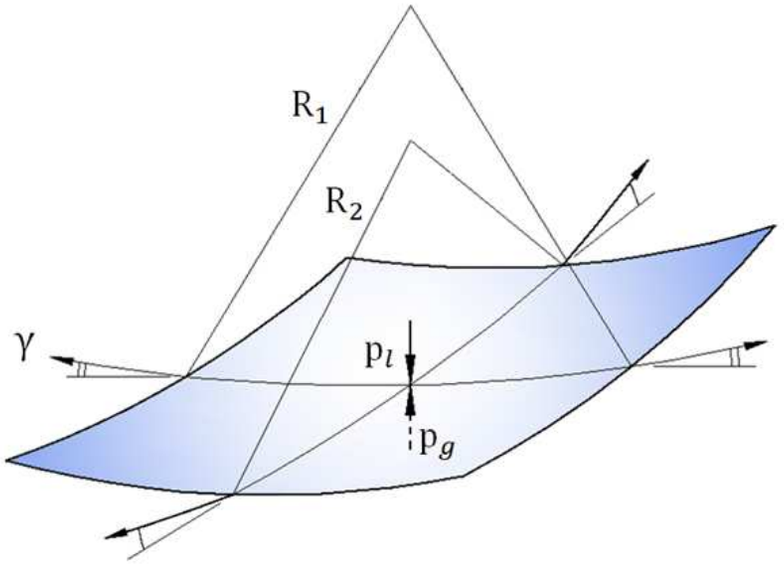


**Figure 5.** Normal pressure balance on an interface (Young-Laplace equation)

Mathematically speaking, it is governed by Young-Laplace equation

$$p_\ell - p_g = \gamma\left(\frac{1}{R_1} + \frac{1}{R_2}\right) \tag{1}$$

where $p_\ell$, $p_g$ are liquid and gas pressures, $\gamma$, the surface tension, $R_1$ and $R_2$ two principal radii of a surface, respectively. Equation (1) can be simply derived from a normal stress balance on an interface [30]. Any physical or chemical variables affecting pressures at the interface are responsible for different surface roughness patterns. The onset and mechanisms of instability are determined from perturbed deformation governed by equation (1) by substituting perturbed liquid and gas pressures. In this work, free surface instability can also be relevantly revealed from the concept of mass conservation, as shown in figures 6(a) and (b). Provided that velocity profiles maintain the same, the free surface is flat. However, the free surface deforms downward, if the mass of the outflow is greater than that of the incoming flow. Since surface deformation is enhanced, the free surface is suffered from instability.

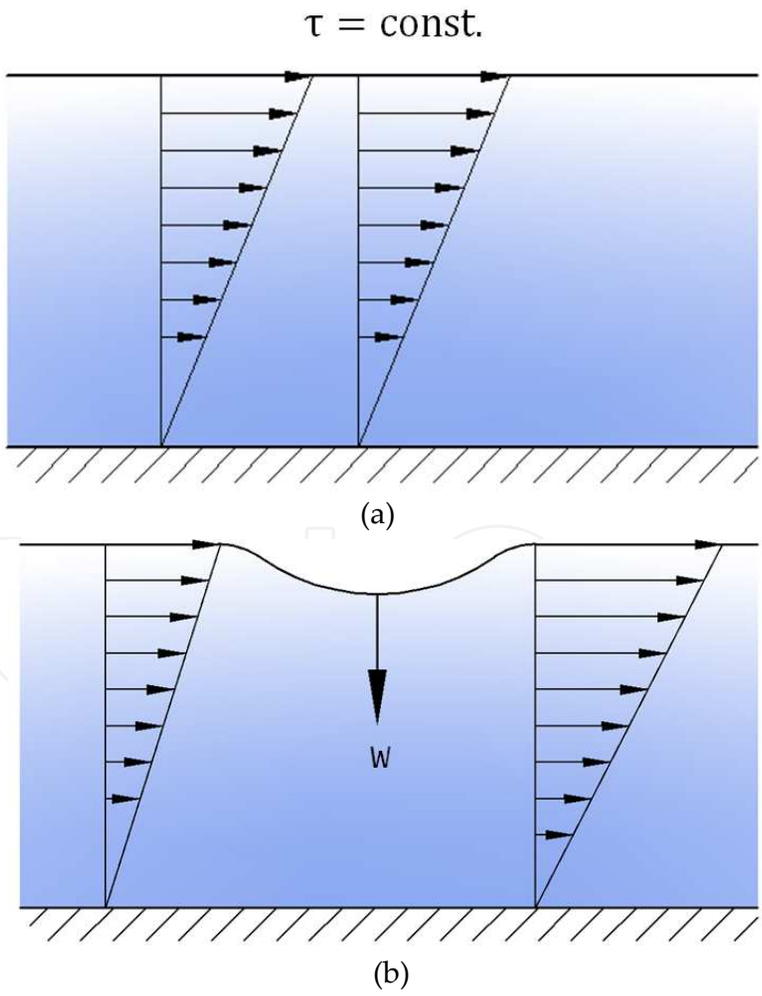


**Figure 6.** The effect of mass flow rate on deformation of a free surface (a) flat free surface, and (b) deformed free surface

The factors affecting surface patterns listed in Table 3 are rigorously described as follows:

## 4. Kelvin-Helmholtz instability

KH instability arises due to difference in velocities between gas and liquid. KH instability is the simplest and widely encountered instability, derived from Young-Laplace equation, where liquid and gas pressures are determined from conservation of mechanical energy (namely, the Bernoulli's equation) with specified constant liquid and gas velocities $U_{\ell 0}$ and $U_{g0}$ far away the location considered. Bernoulli's equation indicates that the lower the velocity is, the higher the pressure is. Provided that deformation is toward the gas, the decrease in perturbed velocity results in an increase in perturbed pressure in the liquid, as illustrated in Figure 7. Opposite phenomenon occurs in gas phase. This results in a further increase in deformation under the action of surface tension. Wavelength for surface deformation can be scaled from equation (1) [1] and given by

$$\lambda_{KH} \sim \frac{\gamma}{\rho_{\ell}(U_{\ell 0} - U_{g0})^2} \tag{2}$$

Wavelength of surface deformation due to KH instability therefore reduces if the difference in velocities between gas and liquid increases. Provided that gas velocity is 10 m/s, the length for roughness in liquid metals is around 10 $\mu m$ within a relevant range of rippling spacing.

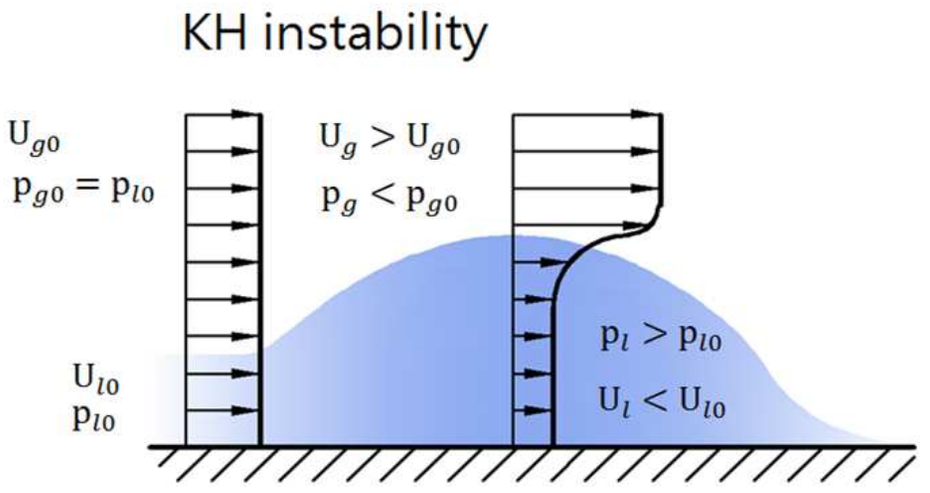


**Figure 7.** Kelvin-Helmholtz instability

## 5. Rayleigh-Taylor instability

RT instability occurs when a heavier liquid overlies a lighter liquid. The pressure involved is hydrostatic pressure, which is a function of gravitational acceleration and the depth location considered. As illustrated in figure 8, the difference in hydrostatic pressures of liquid and gas across a surface with a deformation $\eta$ simply yields

$$p_\ell - p_g = -(\rho_\ell - \rho_g)g\eta \tag{3}$$

Scaling Young-Laplace equation (1) by substituting equation (3) leads to RT instability with the critical wavelength

$$\lambda_{RT} = \sqrt{\frac{\gamma}{g(\rho_\ell - \rho_g)}} \tag{4}$$

Provided that deformation is toward the lighter fluid, a positive perturbed pressure deviated from the base state results. A negative perturbed pressure simultaneously occurs with deformation toward the heavier liquid. Deformation further increases. At later times, initial perturbations grow into spikes of heavier fluid "falling" into lighter fluid and bubble of the lighter fluid "rising" into the heavier fluid. Hence, RT instability has also been stated to occur when the pressure and density gradients are in opposite directions, or a lighter fluid pushes or accelerates a heavier fluid. Equation (4) indicates that an increase in surface tension or decrease in difference in densities across a free surface increases wavelength of ripples.

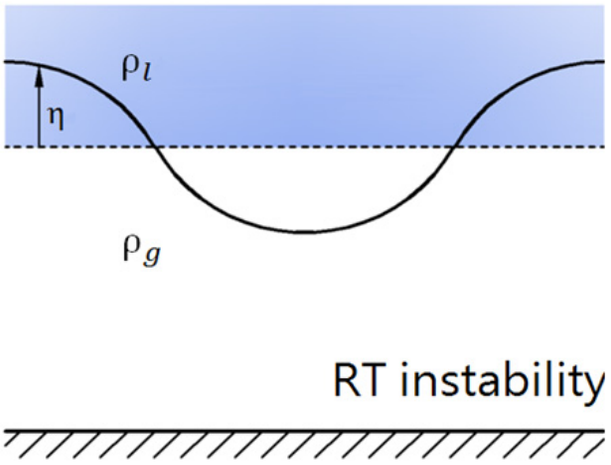


**Figure 8.** Rayleigh-Taylor instability

Acceleration in equation (4) may not be the earth's gravity. RT instability can also occur at an interface separating fluids through which a blast wave has been transmitted from a heavier to a lighter fluid. This instability is Richtmyer-Meshkov instability, often called impulsive or shock-induced RT instability. In high intensity beam welding, the produced shock waves propagate with discontinuities of densities, pressures and velocities in different magnitudes and directions across the free surface. Provided that the interface subject to an oblique shock, it will give rise to complicated instabilities or patterns at the interface. The normal component of the shock generates RM instability, and the parallel component generates KH instability. If a normal acceleration is also present, RT instability occurs.

## 6. Rayleigh's capillary instability

Rayleigh's capillary instability is a crucial factor to understand a bulged or gouging region of surface roughness. The gouged region exhibits an inverse feature of the bulged region.

Rayleigh's capillary instability can be revealed from figure 9. Radius $r_B$ is at a location B near the minimum radius $r_A$. Provided that wavelength of surface deformation is long, curvature $1/R_2 >> 1/R_1$ at location A, as illustrated in figure 9(a). Since liquid pressure is primarily balanced by capillary pressure due to curvature $1/R_2$, a greater liquid pressure is induced by a smaller radius of the cylinder. The positive difference in the pressures thus induces a perturbed flow from locations A to B. The system therefore is unstable and breakups the cylinder into droplets. However, figure 9(b) shows that for deformation with small wavelength, curvature $1/R_1 >> 1/R_2$ at location A. The perturbed pressures at location A therefore decrease and it can be smaller than perturbed pressure at location B, leading to the flow from points B to A, and stabilizing the system.

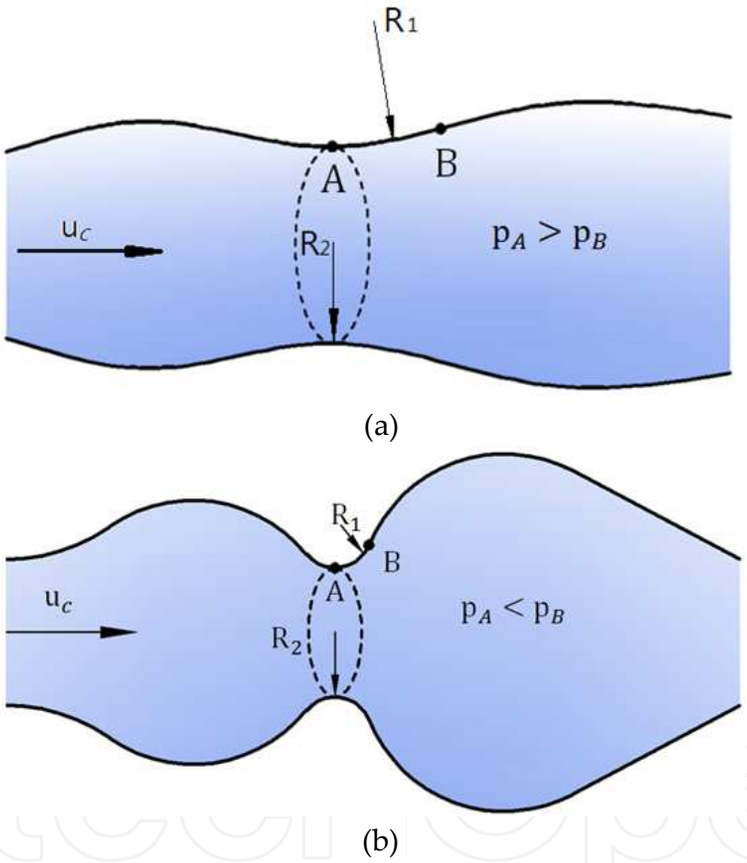


**Figure 9.** Cylinder is unstable for (a) $1/R_2 >> 1/R_1$, and stable for (b) $1/R_1 >> 1/R_2$ at location A

Since the difference in the perturbed pressures at two locations affects instability, the minimum wavelength for onset of instability is the balance between two components of capillary pressure. The critical wavelength thus is of the same order of the radius of the liquid cylinder [31]. Stability of a bead should depend on the boundary conditions at its contact lines on the surface. Gau et al. [32] experimentally found that cylindrical segments for water on hydrophilic stripes with the apparent contact angle less than $90^\circ$ did not break

up into droplets, as would be expected. It displayed long-wavelength instability where all excess fluid gathered into a single bulge on a hydrophilic stripe. Speth and Lauga [33] theoretically confirmed the most unstable wavenumber for the instability —the one which was observed in an experimental setting — decreases to zero when the apparent fluid contact angle reached $90^{\circ}$. The creation of bulges in the experiment corresponded with a zero-wavenumber capillary instability.

## 7. Morphological instability

Morphological instability is a consequence of thermal and metallurgical processes. Surface morphology becomes unstable by decreasing surface tension and increasing constitutional supercooling (namely, $mG_c - G_T > 0$) [34,35], where m is the negative slope of the liquidus line in the phase diagram of a dilute solution, $G_c$ and $G_T$ are negative concentration and positive temperature gradients ahead of the solidification front, respectively. The decreased solute concentration increases liquidus temperature near the solidification front, as illustrated in figures 10(a) and (b), respectively, and revealed from the phase diagram of figure 10(c).

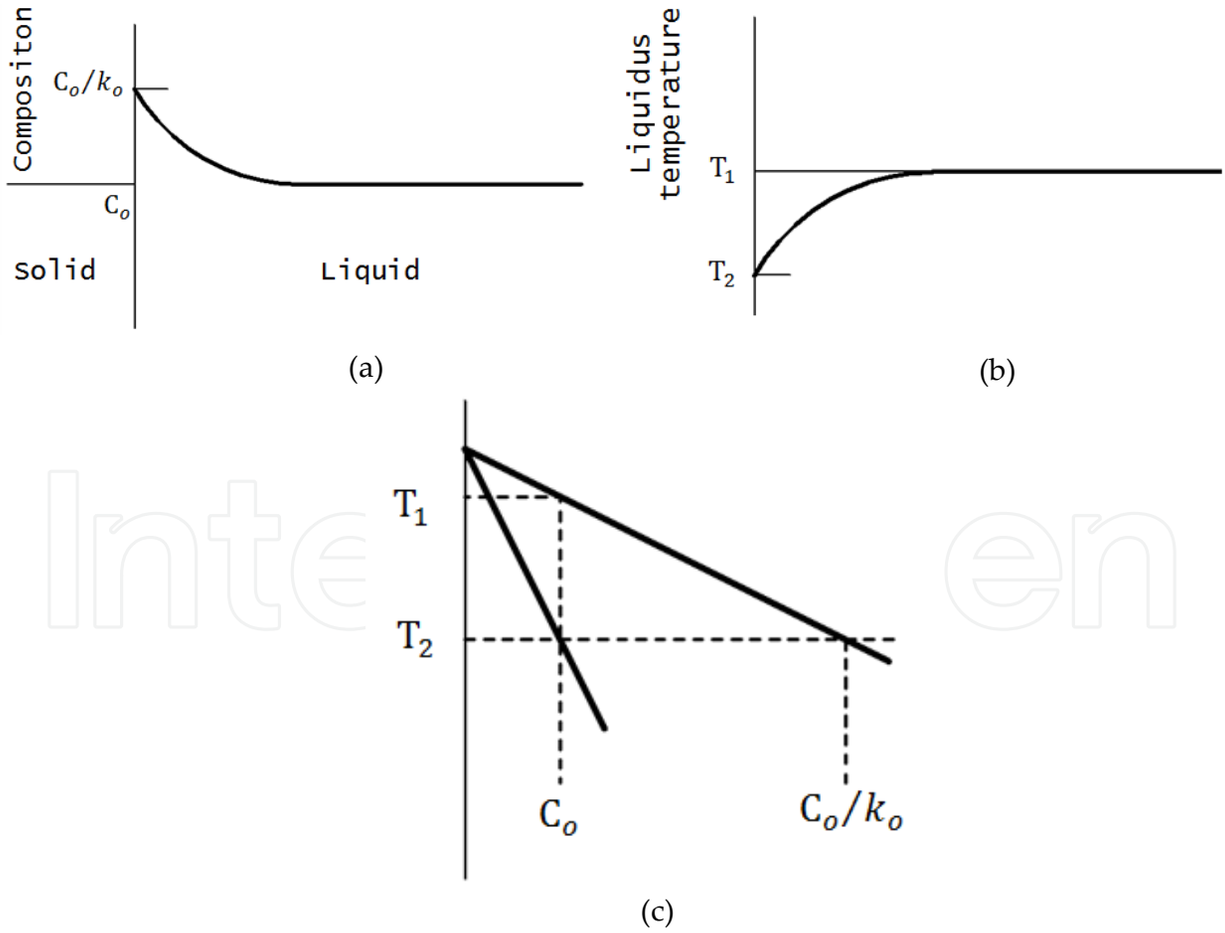


**Figure 10.** (a) Concentration and (b) liquidus temperature profiles ahead of a solidification front, and (c) the corresponding phase diagram

In view of the rapid drop of solute concentration ahead of the freezing front, the actual temperature may be below the liquidus temperature and result in constitutional supercooling or morphological instability, as shown in figure 11. Mathematically speaking, morphological instability can be simply found by considering interfacial temperature governed by Gibbs-Thomson equation [35]

$$T_s - T_m = \frac{\gamma T_m}{\rho h_{s\ell}} \frac{\partial^2 \eta}{\partial x^2} + mC' \tag{5}$$

where $T_S$ , $T_m$, $h_{s\ell}$ are, respectively, interfacial temperature, melting temperature and latent heat for solid-liquid transition. The variations of temperature and concentration at the interface subject to a forward deformation can be expressed by their spatial gradients, $T_s - T_m - mC \sim (G_T - mG_c)\eta_c$ . Scaling equation (5) therefore leads to

$$\lambda_M \sim \sqrt{\frac{\gamma T_m}{\rho h_{s\ell}(mG_c - G_T)}} \tag{6}$$

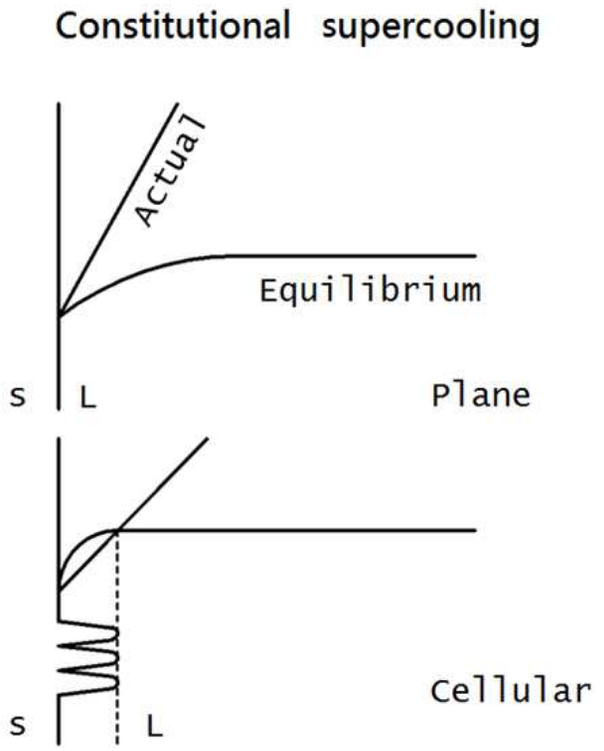


**Figure 11.** Morphological instability due to constitutional supercooling

## 8. Instability due to evaporation

It is well-known that a semi-infinite liquid heated below is susceptible to evaporative instability, as illustrated in figure 12(a). As surface deformation is closer to the bottom surface than the flat surface, temperature at the trough is greater than the equilibrium

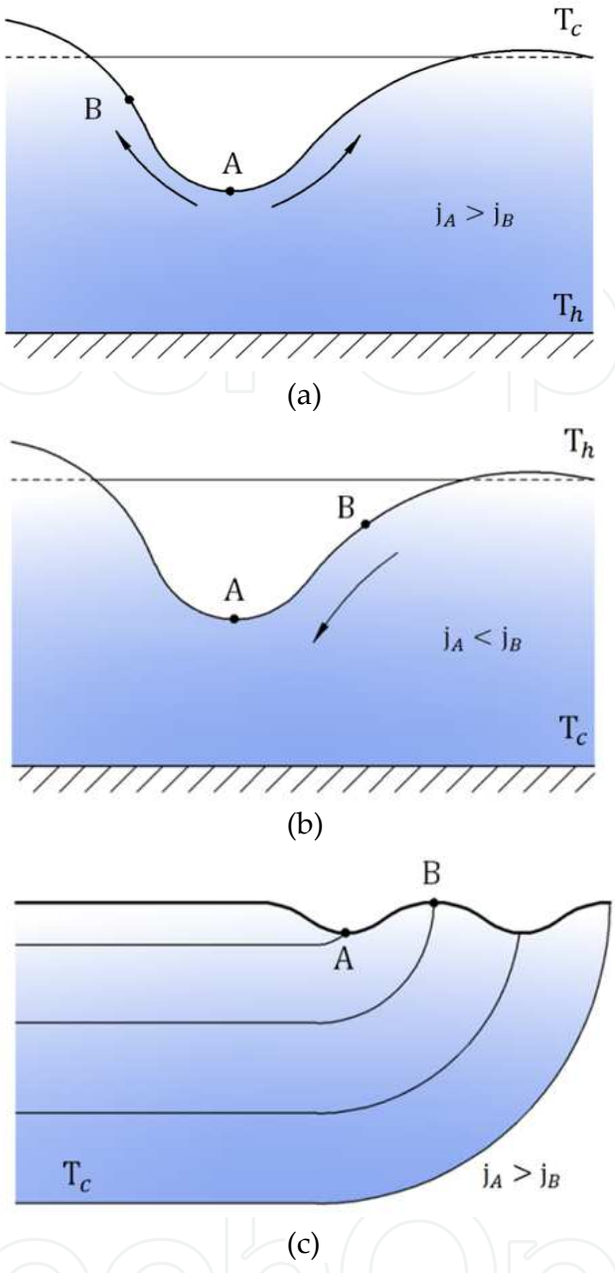


**Figure 12.** Instability due to evaporation for (a) unstable system subject to heating from below, and (b) stable system and (c) unstable system subject to heating from above

temperature, meaning that higher evaporation takes place at the trough than the base state. On the other hand, a deformation away from the bottom surface leads to lower evaporation rate than that at the base state. Liquid pressure therefore increases from the surface trough to crest. The induced flow from the trough to crest thus enhances surface deformation, leading to evaporative instability (referring to figure 6(b)). However, in welding and manufacturing processes, workpieces are irradiated by incident flux at the top surfaces. A liquid heated from above, which is the case opposite to previous figure 12(a), is stable, as illustrated in figure 12(b). In this work, it is found that evaporation may also induce instability subject to base temperature decreasing in radial directions, as illustrated in figure

12(c) [1]. For a typical welding process the isothermal field is in a roughly spherical shape. Provided that surface deforms toward the bottom, temperature at the crest, which is close to the pool edge, can be lower than that at the trough. The decrease in pressures therefore pushes the liquid from the trough to crest and gives rise to instability.

## 9. Thermocapillary instability

All pure liquid metals and alloys containing minor surface active solutes such as O, S, Se, Te, et al. have negative surface tension coefficient ($d\gamma / dT < 0$). As illustrated in figure 13, thermocapillary force balanced by viscous shear stress at the interface is given by

$$\tau = \mu \frac{\partial u_t}{\partial n} = \frac{d\gamma}{dT}\frac{\partial T}{\partial s} \tag{7}$$

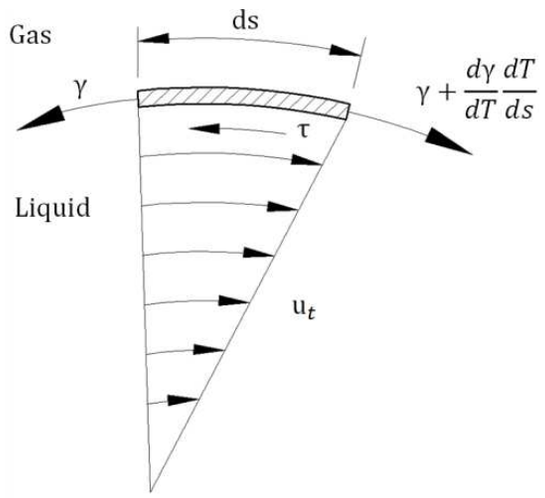


**Figure 13.** Tangential stresses balance between thermocapillary force and shear stress.

A negative surface tension coefficient induces an outward surface flow, provided that surface temperature decreases in the outward direction. Consider an interface to be displaced toward the hot surface at the bottom, as illustrated in figure 14(a). Temperature at the trough thus is hotter than other points on the deformed surface. This results in an outward lateral flow from the trough to crest along the interface. To conserve mass, the perturbed liquid flows downwards and further deforms the interface with speed w (referring to figure 6(b)). The system thus is unstable. The well-accepted interpretation is incorrect. Rather than perturbed downward flow, it is usually interpreted as that instability results from incessant and amplified upward flow accompanying with enhanced energy at the trough due to increased thermocapillary force from the trough to crest [31].

In this work, it is proposed that a free surface heated from above and a negative surface tension coefficient may still cause instability, as illustrated in figure 14(b) [1]. Provided that the surface is strongly deformed toward the bottom, significant heat conduction is transport from the interior to free surface. Enhanced downward thermocapillary surface flow therefore is required to balance horizontal conduction, and results in further deformation. This work also

proposes that thermocapillary instability takes place near the edge of the molten pool, where $d\gamma / dT > 0$ in the presence of surface active solutes in the case similar to the mechanism (see figure 14(a)) provided by Pearson [36], as illustrated in figure 14(c). This is another reason responsible for serious roughness encountered in alloys having surface active solutes [21].

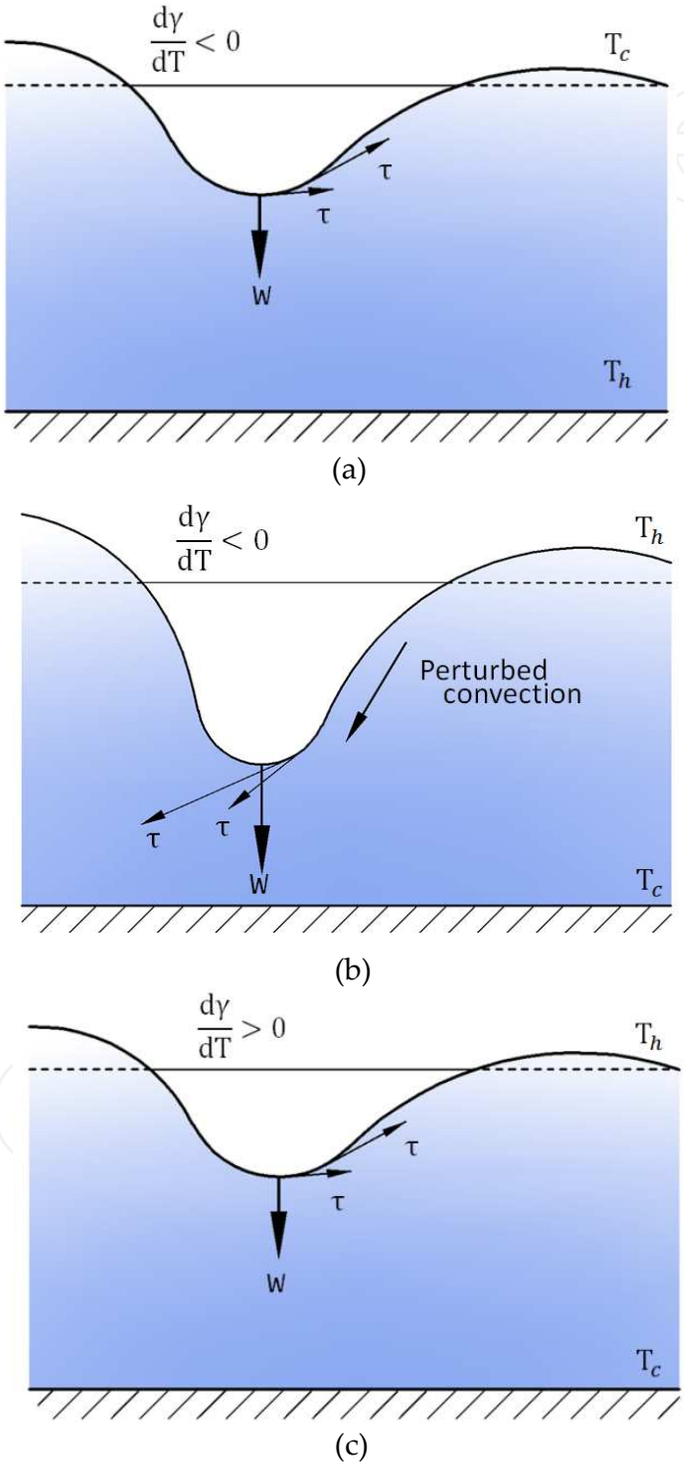


**Figure 14.** Thermocapillary instabilities: (a) heated from below and (b) heated from above with negative surface tension coefficient, and (c) heated from above with positive surface tension coefficient.

## 10. Thermocapillary edge flow

Deformation of the free surface near the solidification front is responsible for rippling or humping. As illustrated in figure 15, an increase in liquid pressure due to a decreased surface flow from the central to rear edge of the pool give rise to deformation of the free surface near the solidification front. Subtracting Young-Laplace equation at two locations which are away and near the edge of the pool surface, and introducing the pressure difference between two locations from Bernoulli's equation,, the amplitude of ripples can be found to be [1,20]

$$\frac{a\gamma}{\rho\alpha^2} = (1 - K_{loss})(\frac{u_c r_m}{\alpha})^2 \tag{8}$$

where the loss coefficient $K_{loss}$ is introduced to account for the energy loss near the pool edge, a, $\alpha$ and $r_m$ are, respectively, roughness amplitude, thermal diffusivity and distance of the rear edge measured from the pool center. Surface speed can be scaled and related to thermocapillary force [37,38]. Based on a typical surface velocity of 1 m/s, pool width of 1 mm and loss coefficient of 0.99, rippling amplitude predicted from equation (8) is around a reasonable value of 10 $\mu m$ .

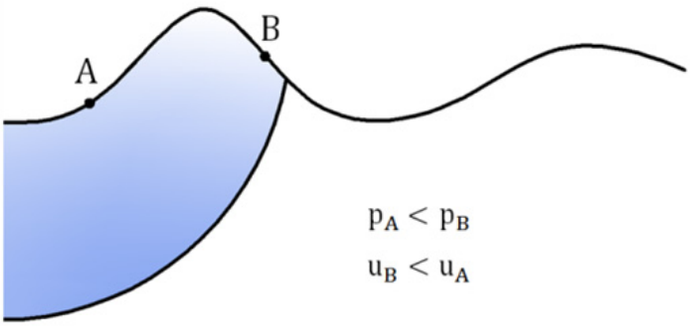


**Figure 15.** Thermocapillary edge flow

## 11. Hydraulic jump

Studying hydraulic jump usually assumes liquid pressure to be hydrostatic pressure. Hydraulic jump occurs if the pressure gradient becomes increasingly adverse as the flow proceeds downstream. As sketched in figure 16(a), an increased liquid height ($h_1 > h_0$) increases hydrostatic force (= pressure x height) against the downward flow, and decreases downward velocity to satisfy conservation of momentum and mass. However, liquid height at the downstream location can also be less than that at the upstream location, as illustrated in figure 16(b). Hydrostatic force decreases whereas velocity increases. Provided that the Froude number, $U_0^2 / gh_0 > 1$, hydraulic jump occurs because of $h_1 / h_0 > 1$ [30]. As Froude number $U_0^2 / gh_0 < 1$, the height ratio $h_1 / h_0 < 1$. Surface tension can also play a role in

hydraulic jump [39], as observed the occurrence of polygonal patterns from breaking axial symmetry of a circular hydraulic jump.

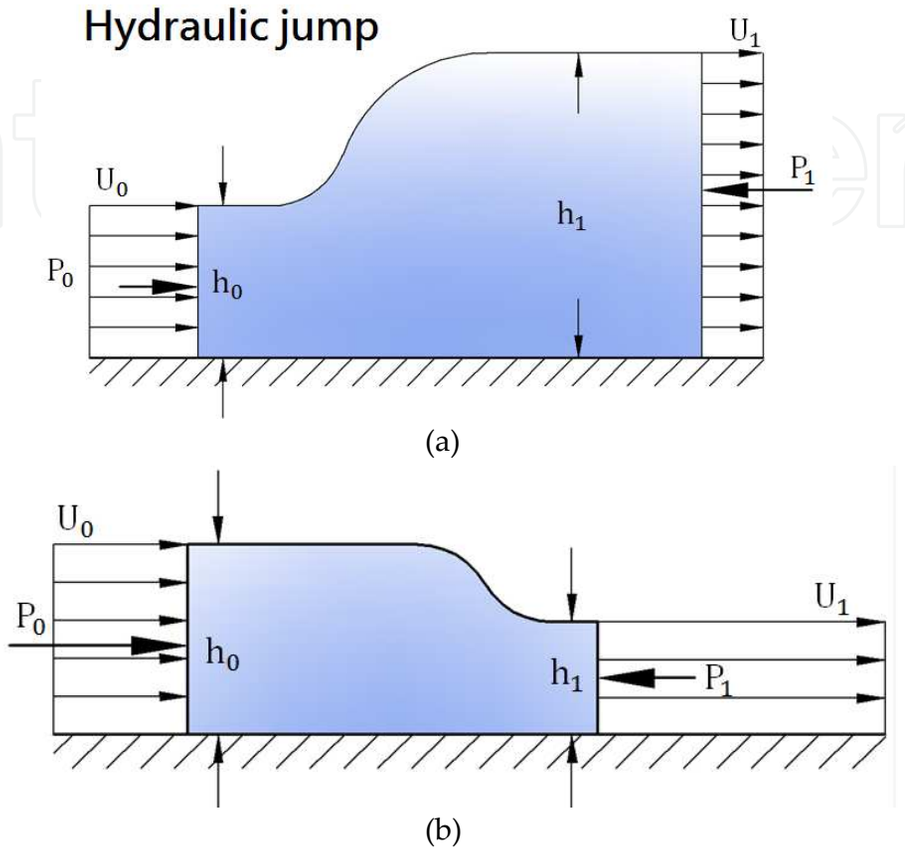


**Figure 16.** Hydraulic jumps with (a) increase and (b) decrease of height at downstream location.

## 12. Fingers

Fingers can be accompanied with hydraulic jump (see figure 4). This is because pressure and density gradients are in opposite directions in the course of splashing, leading to RT instability. Allen [40] was the first to propose that the splashing of a droplet impact on a surface is an example of RT instability, caused by a rapidly decelerating interface. Replacing gravitational acceleration by $u_c / t_c$ in equation (4) and substituting $r_c = n\lambda_{RT}$ from geometrical consideration lead to

$$r_c \sim n\sqrt{\frac{\gamma t_c}{u_c \rho_\ell}} \tag{9}$$

Provided that time is short, equation (9) indicates that radius of the ring-shaped spread is less than wavelength of fingers. The ring-shaped spread thus is free from fingers. On the other hand, larger time results in the ring-shaped spread covered with n fingers.

## 13. Gravitational-electromagnetic instability

In plasma, Rayleigh-Taylor instability can occur because the magnetic field acts as a light fluid supporting a heavy fluid (plasma), [41]. This is because the ion drift velocity $\mathbf{U}_0$ is in the direction of $\mathbf{g} \times \mathbf{B}_0$. If a ripple in plasma develops on the interface as the result of random thermal fluctuations, the drift velocity $\mathbf{U}_0$ will cause the ripple to grow, as sketched in figure 17. Gravitational acceleration $\mathbf{g}$ is in the downward direction. The drift of ions causes a charge to build up on the sides of the ripple, and an electric field develops which changes sign as one goes from crest to trough in the perturbation. The drift $\mathbf{E}' \times \mathbf{B}_0$ is thus always upward in those regions where the surface has moved upward, and downward where it has moved downward. The ripple therefore grows as a result of these properly phased $\mathbf{E}' \times \mathbf{B}_0$ drifts.

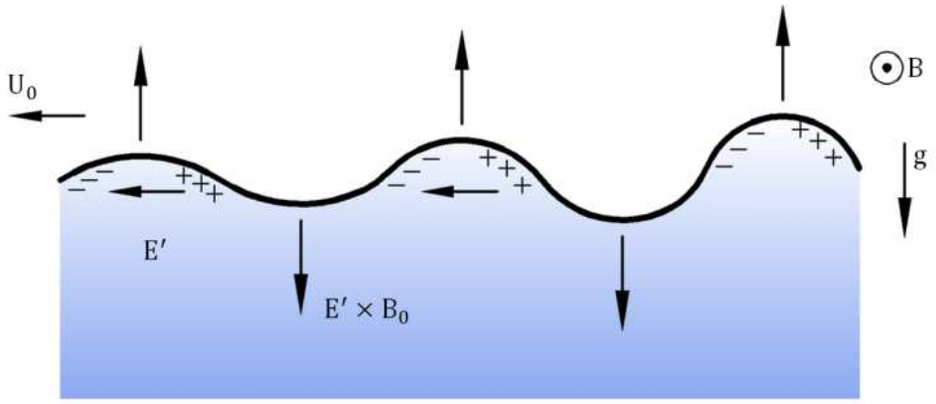


**Figure 17.** Gravitational-electromagnetic instability

## 14. Conclusions

Physical interpretation of bead defects is important and beneficial for controlling quality of welding joint. It involves inter-discipline among different sciences of thermal physics, aerodynamics, electromagnetism, optics and metallurgy, morphology, pattern selection, instabilities, and contact line dynamics. Phase transitions between liquid and gas, and solid and liquid are also included. Spaces and amplitudes of rippling and humping can be effectively revealed from scaling of a force balance between perturbed liquid and gas pressures and surface tension. Any factor which can induce pressure differences or influence surface tension is responsible for specific surface patterns. This study provides a general, relevant and rigorous interpretation of physical mechanisms involved in surface roughness.

## Author details

P. S. Wei
*Department of Mechanical and Electro-Mechanical Engineering,*
*National Sun Yat-Sen University, Kaohsiung, Taiwan, China*

## Acknowledgement

The author is grateful for Mr. Sheng-You Tsai drawing the pictures

## 15. References

[1] Wei, P. S., 2011. Thermal science of weld bead defects- a review, *ASME Journal of Heat Transfer*, 133: 031005

[2] Wei, P. S., Chuang, K.C., Ku, J. S., and DebRoy, T., 2012, Mechanisms of spiking and humping in keyhole welding. *IEEE Transactions on Components, Packaging and Manufacturing Technology* 2: 383-394.

[3] Pedraza, A. J., Guan, Y. F., Fowlkes, J. D., and Smith, D. A., 2004. Nanostructures produced by ultraviolet laser irradiation of silicon. I. rippled structures. *Journal of Vacuum Science and Technology* B 22: 2823-2835.

[4] Soderstrom, E., and Mendez, P. 2006. Humping mechanisms present in high speed welding. *Science and Technology of Welding and Joining* 11: 572-579.

[5] Mendez, P. F., and Eagar, T. W., 2003. Penetration and defect formation in high-current arc welding. *Welding Journal* 82: 296-s to 306-s.

[6] Cho, M. H., and Farson, D. F., 2007. Understanding bead hump formation in gas metal arc welding using a numerical simulation. *Metallurgical and Materials Transactions B* 38: 305-319.

[7] Bäuerle, D., 1996, *Laser Processing and Chemistry,* Springer-Verlag, New York.

[8] Cheever, D. L., and Howden, D. G., 1969. Technical note: nature of weld surface ripples. *Welding Journal* 48: 179-s to 180-s.

[9] D'annessa, A. T., 1970. Sources and effects of growth rate fluctuations during weld metal solidification. *Welding Journal* 49: 41-s to 45-s.

[10] Garland, J. G., and Davies, G. J., 1970. Surface rippling and growth perturbations during weld pool solidification. *Metal Construction and British Welding Journal* 2: 171-175.

[11] Ecer, G. M., Tzavaras, A., Gokhale, A., and Brody, H. D., 1982. Weld pool fluid motion and ripple Formation in pulsed-current GTAW. *Trends in Welding Research in the United States,* (editor David, S. A.), Proceedings of a conference sponsored by the Joining Division of American Society for Metals, New Orleans, Nov. 16-18, 1981, pp.419-442.

[12] Fujimura, K., Ogawa, M., and Seki, M., 1992. Possible mechanism of the roughness formation on a liquid layer caused by a high heat flux. *Fusion Engineering and Design* 19: 183-191.

[13] Ang, L. K., Lau, Y. Y., Gilgenbach, R. M., Spindler, H. L., Lash, J. S., and Kovaleski, S. D., 1998. Surface instability of multipulse laser ablation on a metallic target. *Journal of Applied Physics* 83: 4466-4471.

[14] Bennett, T. D., Grigoropoulos, C. P., and Krajnovich, D. J., 1995. Near-threshold laser sputtering of gold. *Journal of Applied Physics* 77: 849-864.

[15] Lugomer, S. 2007. Micro-fluid dynamics via laser-matter interaction: vortex filament structures, helical instability, reconnection, merging, and undulation. *Physics Letters A* 361: 87-97.

[16] Emel'yanov, V. I., Konov, V. I., Tokarev, V. N., and Seminogov, V. N., 1989. Formation of periodic surface ripples under the action of pulsed carbon dioxide laser radiation on fused silica. *Journal of Optical Society of America* B 6: 104-114.

[17] Weizman, M., Nickel, N. H., Sieber, I, and Yan, B., 2008. Laser-induced self-organization in silicon-germanium thin films. *Journal of Applied Physics* 103: 093536.

[18] Style, R. W., and Wettlaufer, J. S., 2007. Evaporatively driven morphological instability. *Physical Review E* 76: 011602.

[19] Anthony, T. R., and Cline, H. E., 1977. Surface rippling induced by surface-tension gradients during laser surface melting and alloying. *Journal of Applied Physics* 48: 3888-3894.

[20] Wei, P. S., Chang, C. Y., and Chen, C. T., 1996.Surface ripple in electron-beam welding solidification. *ASME Journal of Heat Transfer* 118: 960-969.

[21] Wei, P. S., Chen, Y. H., Ku, J. S., and Ho, C. Y., 2003. Active solute effects on surface ripples in electron-beam welding solidification. *Metallurgical and Materials Transactions B* 34: 421-432.

[22] Birnbaum, M., 1965, Semiconductor Surface Damage Produced by Ruby Lasers, *Journal of Applied Physics*, 36: 3688-3689.

[23] Siegman, A. E., and Fauchet, P. M., 1986. Stimulated Wood's anomalies on laser-illuminated surfaces. *IEEE Journal of Quantum Electronics* QE-22: 1384-1403.

[24] Bradstreet, B. J., 1968. Effect of surface tension and metal flow on weld bead formation. *Welding Journal*, 47: 314-s to 322-s.

[25] Gratzke, U., Kapadia, P. D., Dowden, J., Kroos, J., and Simon, G., 1992. Theoretical approach to the humping phenomenon in welding processes. *Journal of Physics D: Applied Physics* 25: 1640-1647.

[26] Albright, C. E., and Chiang, S., 1988. High-speed laser welding discontinuities. *Journal of Laser Applications* 1: 18-24.

[27] Kumar, A., and DebRoy, T., 2006. Toward a unified model to prevent humping defects in gas tungsten arc welding. *Welding Journal* 85: 292-s to 304-s.

[28] Tytkin, Yu. M., Ryazantsev, O. V., and Chuvilo, V. N., 1981. The mechanism of formation of a coarse flaky surface of weld metal in welding under high-power conditions. *Svar. Proiz.* 2: 4-5 (pp.3-5).

[29] Shimada, W., and Hoshinouchi, S., 1982. A study on bead formation by low pressure TIG arc and prevention of under-cut bead. *Transactions of the Japan Welding Society* 51: 280-286.

[30] Li, W. H., and Lam, S. H., 1964, *Principles of Fluid Mechanics,* Addison-Wesley, Reading, Mass., 1964.

[31] Miller, C. A., and Neogi, P., 1985, *Interfacial Phenomena, Equilibrium and Dynamic Effects,* Marcel Dekker, New York.

[32] Gau, H., Herminghaus, S., Lenz, P., and Lipowsky, R., 1999. Liquid morphologies on structured surfaces: from microchannels to microchips. *Science* 283: 46-49.

[33] Speth, R. L., and Lauga, E., 2009. Capillary instability on a hydrophilic stripe. *New Journal of Physics* 11: 075024.

[34] Rutter, J. W., and Chalmers, B., 1953. A prismatic substructure formed during solidification of metals. *Canadian Journal of Physics* 31: 15-39.
[35] Mullins, W. W., and Sekerka, R. F., 1964. Stability of a planar interface during solidification of a dilute binary alloy. *Journal of Applied Physics* 35: 444-451.
[36] Pearson, J. R. A., 1958. On convection cells induced by surface tension. *Journal of Fluid Mechanics* 4: 489-500.
[37] Ostrach, S., 1982, Low-Gravity Fluid Flows, *Annual Review of Fluid Mechanics* 14: 313-345.
[38] Wei, P. S., Liu, H. J., and Lin, C. L., 2012, Scaling weld or melt pool shape induced by thermocapillary convection, *International Journal of Heat and Mass Transfer* 55: 2328-2337.
[39] Ellegaard, C., Hansen, A. E., Haaning, A., Hansen, K., Marcussen, A., Bohr, T., Hansen, J. L., and Watanabe, S., 1998. Creating corners in kitchen sinks. *Nature* 392: 767-768.
[40] Allen, R. F., 1975. The role of surface tension in splashing. *Journal of Colloid and Interface Science* 51: 350-351.
[41] Chen, F. F., 1974, *Introduction to Plasma Physics,* Plenum Press, New York